

Bistability and hysteresis of dipolar dynamos generated by turbulent convection in rotating spherical shells

R. D. SIMITEV¹ and F. H. BUSSE²

¹ *Department of Mathematics, University of Glasgow, Glasgow G12 8QW, UK*

² *Institute of Physics, University of Bayreuth, Bayreuth D-95440, Germany*

PACS 91.25.Cw – Origins and models of the magnetic field; dynamo theories

PACS 92.60.hk – Convection, turbulence, and diffusion

PACS 47.20.Ky – Nonlinearity, bifurcation, and symmetry breaking

Abstract. - Bistability and hysteresis of magnetohydrodynamic dipolar dynamos generated by turbulent convection in rotating spherical fluid shells is demonstrated. Hysteresis appears as a transition between two distinct regimes of dipolar dynamos with rather different properties including a pronounced difference in the amplitude of the axisymmetric poloidal field component and in the form of the differential rotation. The bistability occurs from the onset of dynamo action up to about 9 times the critical value of the Rayleigh number for onset of convection and over a wide range of values of the ordinary and the magnetic Prandtl numbers including the value unity.

R. D. Simitev and F. H. Busse, 2009, Europhys. Lett., 85, 19001

doi: 10.1209/0295-5075/85/19001

Introduction. – An arbitrary weak magnetic field may either decay or be amplified by the motion of an electrically conducting fluid. The latter case is called dynamo effect and it is believed to be responsible for the magnetic fields of cosmic objects including the sun and most planets [1, 2]. The dynamo effect of turbulent convection in rotating spherical fluid shells has received much attention in recent years [3, 4] because it is the basic model for the generation of the magnetic fields of the Earth and other planets. Many numerical studies following [5, 6] have attempted a direct comparison with geomagnetic observations and have been remarkably successful in reproducing some of the main properties of the geomagnetic field [7, 8] while others have focused on more systematic explorations of the computationally accessible parameter space e.g. [9–13]. Dynamos obtained through numerical simulations are usually turbulent and it is assumed that their time averaged properties are independent of the initial conditions once the computations have run for a sufficiently long time. In contrast to this assumption we wish to demonstrate in this Letter that bistability and hysteresis of convection-driven turbulent dynamos occur in a wide region of the parameter space. The co-existence of two distinct turbulent attractors is also of general interest. In contrast to the common bistability associated with a subcritical bifurcation from a laminar to a turbu-

lent attractor, the co-existence of two turbulent attractors is a rare phenomenon in fluid dynamics [14, 15] and magnetohydrodynamics. Subcritical onset of dynamo action is a rather common phenomenon [16–18] and such is hysteresis between non-magnetic and dynamo states. But co-existence and hysteresis between two fully-developed chaotic dynamo states far above onset are, to our knowledge, reported here for the first time. That multiple turbulent states are more likely to occur in hydromagnetic dynamos than in non-magnetic flows is perhaps not surprising because of the additional degrees of freedom offered by the magnetic field.

Formulation. – We consider a spherical fluid shell of thickness d rotating with a constant angular velocity Ω . The existence of a static state is assumed with a temperature distribution $T_S = T_0 - \beta d^2 r^2 / 2$ and a gravity field in the form $\mathbf{g} = -d\gamma \mathbf{r}$, where r is the length of the position vector with respect to the center of the sphere. This form of temperature profile alludes to the possibility that at least a fraction of the energy available to planetary dynamos is due to radiogenic heat release. In addition to d , we use the time d^2/ν , the temperature $\nu^2/\gamma\alpha d^4$ and the magnetic flux density $\nu(\mu\rho)^{1/2}/d$ as scales for the dimensionless description of the problem where ν denotes the kinematic viscosity of the fluid, κ its thermal diffusivity,

ρ its density and μ its magnetic permeability. In common with most other simulations of Earth and planetary dynamos [4, 7], we assume the Boussinesq approximation implying a constant density ρ except in the gravity term where its temperature dependence is taken into account with $\alpha \equiv -(\mathrm{d}\rho/\mathrm{d}T)/\rho = \text{const}$. The equations of motion for the velocity vector \mathbf{u} , the heat equation for the deviation Θ from the static temperature distribution, and the equation of induction for the magnetic flux density \mathbf{B} are then given by

$$\nabla \cdot \mathbf{u} = 0, \quad \nabla \cdot \mathbf{B} = 0, \quad (1a)$$

$$(\partial_t + \mathbf{u} \cdot \nabla) \mathbf{u} + \tau \mathbf{k} \times \mathbf{u} = -\nabla \pi + \Theta \mathbf{r} + \nabla^2 \mathbf{u} + \mathbf{B} \cdot \nabla \mathbf{B}, \quad (1b)$$

$$P(\partial_t \Theta + \mathbf{u} \cdot \nabla \Theta) = R \mathbf{r} \cdot \mathbf{u} + \nabla^2 \Theta, \quad (1c)$$

$$\nabla^2 \mathbf{B} = P_m (\partial_t \mathbf{B} + \mathbf{u} \cdot \nabla \mathbf{B} - \mathbf{B} \cdot \nabla \mathbf{u}), \quad (1d)$$

where all gradient terms in the equation of motion have been combined into $\nabla \pi$. The dimensionless parameters in our formulation are the Rayleigh number R , the Coriolis number τ , the Prandtl number P and the magnetic Prandtl number P_m ,

$$R = \frac{\alpha \gamma \beta d^6}{\nu \kappa}, \quad \tau = \frac{2\Omega d^2}{\nu}, \quad P = \frac{\nu}{\kappa}, \quad P_m = \frac{\nu}{\lambda}, \quad (2)$$

where λ is the magnetic diffusivity. Being solenoidal vector fields \mathbf{u} and \mathbf{B} can be represented uniquely in terms of poloidal and toroidal components,

$$\mathbf{u} = \nabla \times (\nabla v \times \mathbf{r}) + \nabla w \times \mathbf{r}, \quad (3a)$$

$$\mathbf{B} = \nabla \times (\nabla h \times \mathbf{r}) + \nabla g \times \mathbf{r}. \quad (3b)$$

We assume fixed temperatures at $r = r_i \equiv 2/3$ and $r = r_o \equiv 5/3$ and stress-free rather than no-slip boundary conditions in order to approach, at least to some extent, the extremely low values of viscosity believed to be appropriate to planetary cores [6],

$$v = \partial_{rr}^2 v = \partial_r(w/r) = \Theta = 0. \quad (4)$$

For the magnetic field we assume electrically insulating boundaries at $r = r_i$ and $r = r_o$ such that the poloidal function h matches the function $h^{(e)}$ which describes the potential fields outside the fluid shell,

$$g = h - h^{(e)} = \partial_r(h - h^{(e)}) = 0 \text{ at } r = r_i, r_o. \quad (5)$$

The radius ratio $r_i/r_o = 0.4$ is slightly larger than that appropriate for the Earth's liquid core. This is a standard formulation of the spherical convection-driven dynamo problem [2–4] for which an extensive collection of results already exists [10, 11, 19, 20]. The results reported below are not strongly model dependent. In particular, dynamos with stress-free and with no-slip velocity boundary conditions as well as with different modes of energy supply are known to have comparable energy densities and symmetry properties (see fig. 15 of [4]). Furthermore,

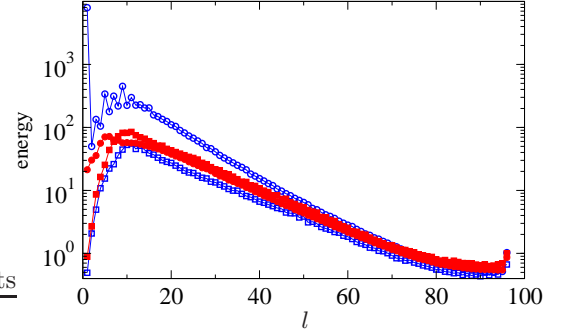


Fig. 1: (color online) Resolution test: Time-averaged spectra of magnetic (circles) and kinetic (squares) energy as a function of the harmonic degree l for the two cases shown in fig. 2. The MD case is given in blue and indicated by empty symbols and the FD case is given in red and indicated by solid symbols.

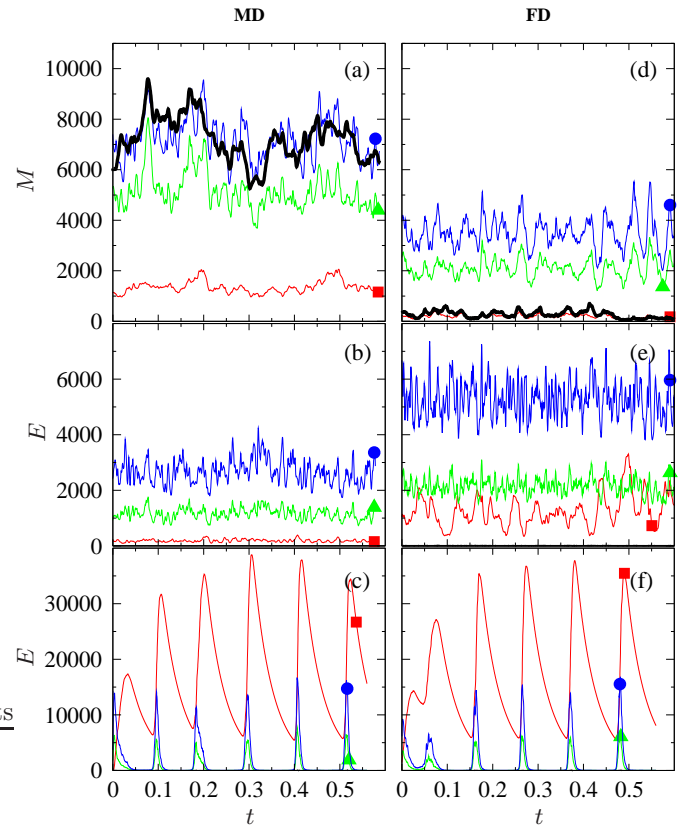


Fig. 2: (color online) Time series of two different chaotic attractors are shown - a MD (left column (a,b)) and a FD dynamo (right column (d,e)) both in the case $R = 3.5 \times 10^6$, $\tau = 3 \times 10^4$, $P = 0.75$ and $P_m = 1.5$. The top two panels (a,d) show magnetic energy densities. The rest of the panels show kinetic energy densities in the presence of magnetic field (b,e) and after the magnetic field is removed (c,f). The component \bar{X}_p is shown by thick solid black line, while \bar{X}_t , \tilde{X}_p , and \tilde{X}_t are shown by thin red, green and blue lines, respectively, and they are also indicated by squares, triangles and circles, respectively. X stands for either M or E .

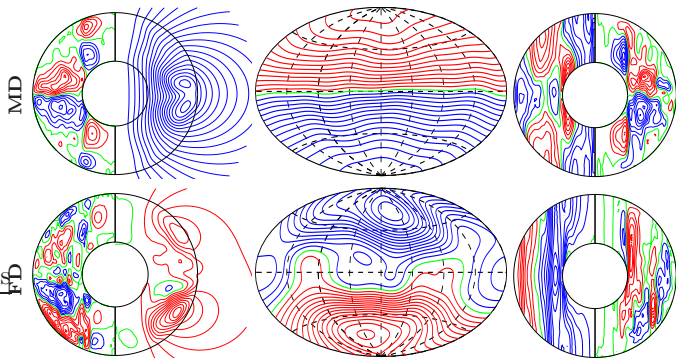


Fig. 3: (color online) A **MD** and a **FD** dynamo both in the case $R = 3.5 \times 10^6$, $\tau = 3 \times 10^4$, $P = 0.75$ and $P_m = 1.5$. Each circle of the leftmost column shows meridional lines of constant \overline{B}_φ in the left half and of $r \sin \theta \partial_\theta \overline{h} = \text{const.}$ in the right half. The middle column shows lines of constant B_r at $r = r_o + 1.3$. Each circle of the rightmost column shows meridional lines of constant \overline{u}_φ in the left half and of $r \sin \theta \partial_\theta \overline{v}$ in the right half.

aiming to retain a general physical perspective, we intentionally use a minimal number of physical parameters including only those of primary importance for stellar and planetary applications.

Equations of motion for the scalar fields v , w , are obtained by taking $\mathbf{r} \cdot \nabla \times \nabla \times$ and $\mathbf{r} \cdot \nabla \times$ of equation (1b) and equations for g and h are obtained by taking $\mathbf{r} \cdot \nabla \times$ and $\mathbf{r} \cdot$ of equation (1d). These equations are solved numerically by a pseudo-spectral method as described in [21] based on expansions of all dependent variables in spherical harmonics for the angular dependences and in Chebychev polynomials for the radial dependence. Typically, calculations are considered decently resolved when the spectral power of kinetic and magnetic energy drops by more than a factor of 100 from the spectral maximum to the cut-off wavelength [9]. A minimum of 41 collocation points in the radial direction and spherical harmonics up to the order 96 have been used in all cases reported here which provides adequate resolution as demonstrated in fig. 1 for two typical dynamo solutions. The dynamo solutions are characterized by their magnetic energy densities,

$$\begin{aligned} \overline{M}_p &= \frac{1}{2} \langle |\nabla \times (\nabla \overline{h} \times \mathbf{r})|^2 \rangle, & \overline{M}_t &= \frac{1}{2} \langle |\nabla \overline{g} \times \mathbf{r}|^2 \rangle, \\ \widetilde{M}_p &= \frac{1}{2} \langle |\nabla \times (\nabla \widetilde{h} \times \mathbf{r})|^2 \rangle, & \widetilde{M}_t &= \frac{1}{2} \langle |\nabla \widetilde{g} \times \mathbf{r}|^2 \rangle, \end{aligned}$$

where $\langle \cdot \rangle$ indicates the average over the fluid shell and \overline{h} refers to the axisymmetric component of h , while \widetilde{h} is defined by $\widetilde{h} = h - \overline{h}$. The corresponding kinetic energy densities \overline{E}_p , \overline{E}_t , \widetilde{E}_p and \widetilde{E}_t are defined analogously with v and w replacing h and g .

Results. — All solutions reported below are turbulent and typical examples of the variations in time of the energy densities are shown in fig. 2. Apart from the obvious quantitative difference, an essential qualitative change in

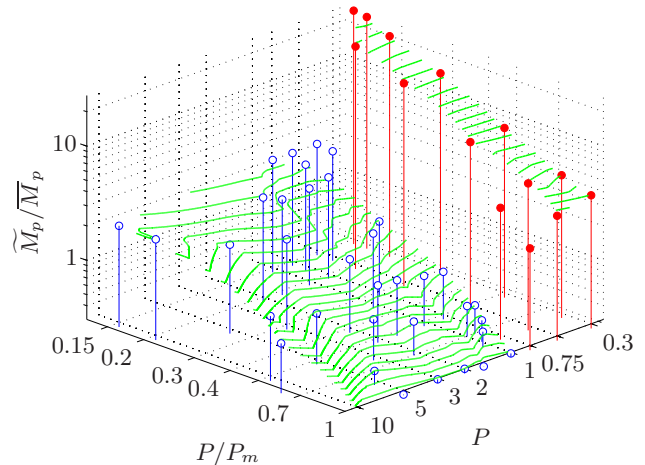


Fig. 4: (color online) The ratio $\widetilde{M}_p / \overline{M}_p$ of dynamo solutions as a function of P and P/P_m at $R = 3.5 \times 10^6$, $\tau = 3 \times 10^4$. Full red and empty blue circles indicate **FD** and **MD** dynamos, respectively. The surface is intentionally left broken near the transition where it is multi-valued as discussed in text.

the balance of magnetic energy components is observed. The axisymmetric poloidal component \overline{M}_p is dominant in the case shown in fig. 2(a,b) while it has a relatively small contribution in the case of fig. 2(d,e) with the corresponding differences in the structure of the magnetic field shown in fig. 3. This observation is in accord with the claim made in [11, 20, 22] that, quite generally, two regimes of dipolar dynamos can be distinguished, namely those with $\widetilde{M}_p < \overline{M}_p$ (regime **MD**, "Mean Dipole") and those with $\widetilde{M}_p > \overline{M}_p$ (regime **FD**, "Fluctuating Dipole"). The transition between the regimes is shown in fig. 4 as a function of the ordinary Prandtl number P and of the ratio P/P_m in the case of fixed $\tau = 3 \times 10^4$ and $R = 3.5 \times 10^6$. The transition between the two distinct turbulent dynamo attractors is not gradual, but has the character of an abrupt jump after a critical parameter value is surpassed as discussed below. All solutions included in fig. 4 have a predominantly dipolar character with the ratio $\overline{M}_p^{\text{dip}} / \overline{M}_p$ in the ranges $[0.95, 1]$ for **MD** dynamos and $[0.45, 0.72]$ for **FD** dynamos. Although, the **FD** dynamos feature an increased contribution of higher multipoles they are still of geophysical relevance [20, 22]. At values of the ordinary and magnetic Prandtl numbers somewhat lower than those included in fig. 4, however, hemispherical and quadrupolar dynamos become predominant.

We note that the two solutions in fig. 2 and fig. 3 are obtained at identical parameter values and thus the chaotic attractors **MD** and **FD** co-exist in this case. Varying P and P_m demonstrates an extended region of this co-existence. In fact, the transition between the **MD** and **FD** dynamos is achieved via hysteresis loops as illustrated in fig. 5 for $\tau = 3 \times 10^4$. When an **MD** dynamo is used as initial data and the Prandtl number P is decreased,

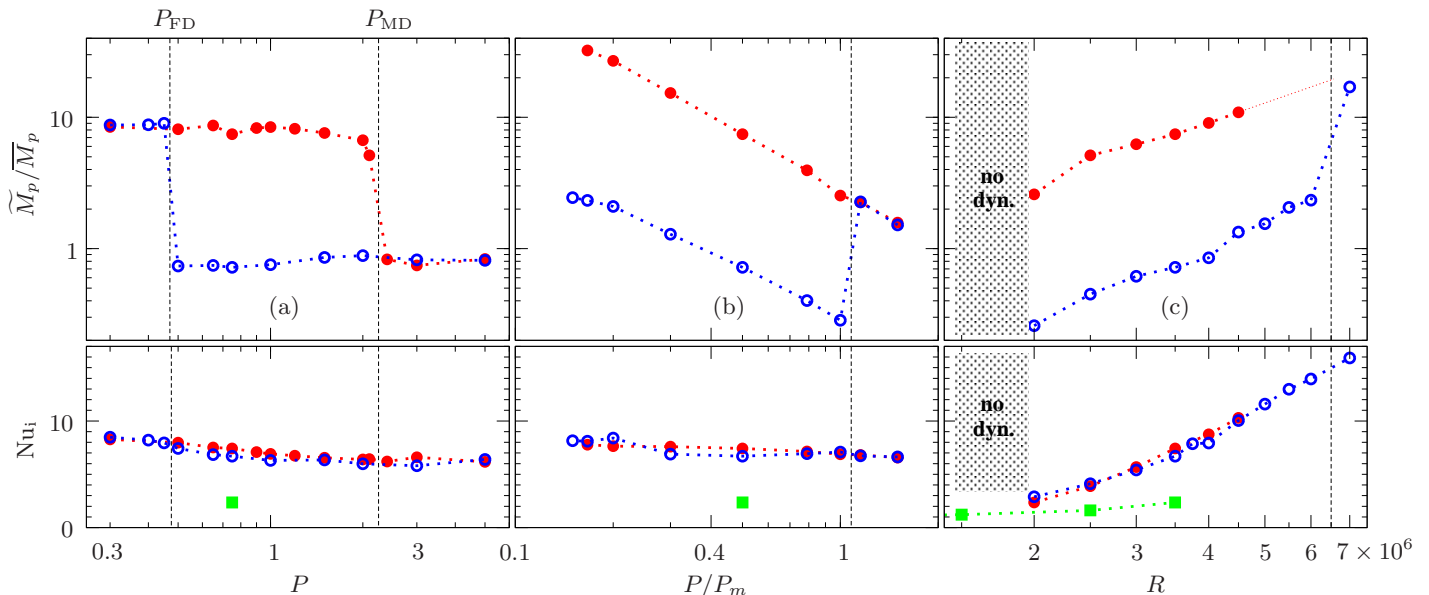


Fig. 5: (color online) The upper row shows the hysteresis effect in the ratio $\widetilde{M}_p/\overline{M}_p$ at $\tau = 3 \times 10^4$ (a) as a function of the Prandtl number in the case of $R = 3.5 \times 10^6$, $P/P_m = 0.5$; (b) as a function of the ratio P/P_m in the case of $R = 3.5 \times 10^6$, $P = 0.75$ and (c) as a function of the Rayleigh number in the case $P = 0.75$, $P_m = 1.5$. Full red and empty blue circles indicate **FD** and **MD** dynamos, respectively. The critical value of R for the onset of thermal convection for the cases shown in (c) is $R_c = 659145$. A transition from **FD** to **MD** dynamos as P/P_m is decreased in (b) is expected, but is not indicated owing to lack of data. The lower row shows the value of the Nusselt number at $r = r_i$ for the same dynamo cases. Values for non-magnetic convection are indicated by green squares for comparison.

solutions remain in regime **MD** until the critical value $P_{\text{FD}} \approx 0.5$ is reached at which point an abrupt jump transition to the **FD** regime occurs. When a **FD** dynamo is used as initial condition and P is increased the reverse transition occurs at the critical value $P_{\text{MD}} \approx 2.2$ as seen in fig. 5(a). Similarly, coexisting attractors are found as a function of the ratio P/P_m for $P/P_m < 1$ and as a function of the Rayleigh number above the onset of dynamo action as seen in figs. 5(b) and (c), respectively. The solutions of the hysteresis loops have been computed for up to at least 3 magnetic diffusion times. No evidence for a transient nature of any case has been found. In fact, in cases beyond the boundaries of the hysteresis loop the transition from **MD** to **FD** regimes or vice versa takes typically only 0.15 magnetic diffusion times. One may notice that the hysteresis loop in the direction of decreasing values of P/P_m in fig. 5(b) is incomplete. We expect a transition from **FD** to **MD** dynamos to occur at sufficiently low values of P/P_m , but we are presently unable to demonstrate it because of the high computational costs of dynamo simulations in this region of the parameter space.

The bistability of convection driven dynamos is the result of two different ways in which the magnetic field damps the differential rotation. In the **MD** dynamos the differential rotation generated by Reynolds stresses of the convection columns is eliminated almost entirely by the strong mean magnetic field as shown in figs. 2(b) and 3. Only a zonal thermal wind caused by latitudinal variations

of the temperature remains as is typical for high Prandtl number dynamos [11]. Because of the strong magnetic field the amplitude of convection is also reduced in comparison with the maximum value that it reaches in the absence of a magnetic field. In the case of **FD** dynamos the differential rotation is still diminished, but its alignment with coaxial cylindrical surfaces is preserved. The amplitude of convection is now more strongly fluctuating, but is larger on average than in the case of the **MD** dynamos. In this way **FD** and **MD** dynamos manage to carry very nearly the same heat transport as is evident from fig. 5. This heat transport by far exceeds the time average of heat transport found in the absence of a magnetic field. Figure 2(c,f) demonstrates that the same type of convection in the form of turbulent relaxation oscillations [19] is generated when the Lorentz force is dropped from the equations of motion.

While the **MD** dynamos are non-oscillatory with limited fluctuations of their axisymmetric components about their time average, the **FD** dynamos usually oscillate in an irregular manner. A rather pure example of such oscillations is shown in fig. 6. The dipolar oscillations of **FD** dynamos can be understood in terms of Parker dynamo waves [20]. In general, however, the oscillations are much less regular and involve considerable contributions of quadrupolar components.

Conclusion. – We have demonstrated the coexistence of two well-distinguishable chaotic attractors in

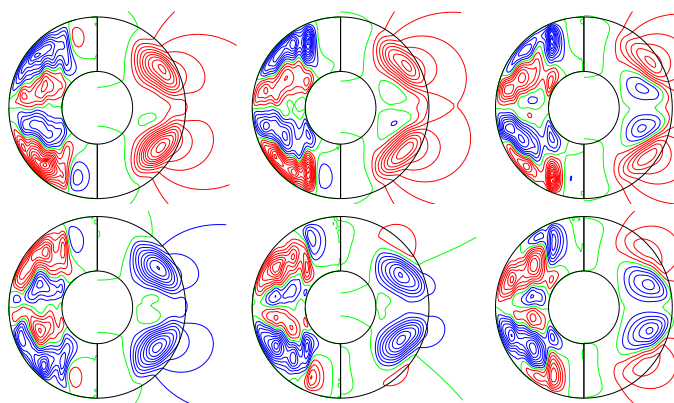


Fig. 6: (color online) A half period of dipolar oscillations in the **FD** case $R = 3.5 \times 10^6$, $\tau = 3 \times 10^4$, $P = 0.75$ and $P_m = 0.65$. The same fields as in the first column of fig. 3 are shown. Plots follow clockwise from upper left with a step $\Delta t = 0.0042$.

a turbulent system over a sizable region of the parameter space. The hysteresis loops occur within the ranges $P \in (0.5, 2.2)$ and $P/P_m < 1$ for the value of τ used here and from onset of dynamo action to at least $9 \times R_c$, where R_c is the critical value for onset of convection. This range is of importance since $P = 1$ is used in most simulations of convection-driven dynamos in rotating spheres [4, 7]. The reason for this is that in comparisons with geomagnetic observations diffusivities such as ν and κ are interpreted as eddy diffusivities which are supposed to represent the effects of the numerically unresolved scales of the turbulent velocity field. Since the diffusion of heat and momentum owing to the small scale turbulence is similar, eddy diffusivities are regarded as equal with the consequence $P = 1$.

Dynamo states similar to **MD** and **FD** dynamos have been obtained previously. A transition between such two states as a function of the Rayleigh number, R , has been reported in [22] where no-slip boundary conditions have been used. A hysteresis phenomenon was not found by these authors. In a later paper [13] a particular case of bistability has been mentioned, but no further discussion was given. Transitions between states similar to **MD** and **FD** dynamos as a function of P or P/P_m caused by the changing strength of the inertial forces have been reported in [11, 23]. In the simulations of [13, 22] and [23] no-slip boundary conditions for the velocity field have been employed and it is of interest to investigate whether, as we expect, the hysteresis phenomenon persists as the velocity boundary conditions and the heating model are changed. Simulations of convection-driven dynamos with no-slip boundary conditions and driven by a basal heat flux are underway and will be reported in a future paper.

While the possibility of hysteretic behavior of planetary dynamos in response to slow changes in their properties is of considerable interest, it will be difficult to obtain observational evidence for such a phenomenon because of

the long time scale of magnetic diffusion. It is important, however, to be aware of the bistability phenomenon in the interpretation of numerical dynamo simulations.

REFERENCES

- [1] RÜDIGER G. and HOLLERBACH R., *The Magnetic Universe: Geophysical and Astrophysical Dynamo Theory* (Wiley-VCH) 2004.
- [2] DORMY E. and SOWARD A., (Editors) *Mathematical Aspects of Natural Dynamos* (CRC Press) 2007.
- [3] BUSSE F. H., *Annu. Rev. Fluid Mech.*, **32** (2000) 383.
- [4] KONO M. and ROBERTS P., *Rev. Geophys.*, **40** (2002) 1013.
- [5] GLATZMAIER G. and ROBERTS P., *Nature*, **377** (1995) 203.
- [6] KUANG W. and BLOXHAM J., *Nature*, **389** (1997) 371.
- [7] DORMY E., VALET J.-P. and COURTILLOT V., *Geochem. Geophys. Geosyst.*, **1** (2000) 2000GC000062.
- [8] KUTZNER C. and CHRISTENSEN U., *Geophys. J. Int.*, **157** (2004) 1105.
- [9] CHRISTENSEN U., OLSON P. and GLATZMAIER G., *Geophys. J. Int.*, **138** (1999) 393.
- [10] GROTE E., BUSSE F. H. and TILGNER A., *Phys. Earth Planet. Inter.*, **117** (2000) 259.
- [11] SIMITEV R. and BUSSE F. H., *J. Fluid Mech.*, **532** (2005) 365.
- [12] TAKAHASHI F. and MATSUSHIMA M., *Phys. Fluids*, **7** (2005) 076601.
- [13] CHRISTENSEN U. and AUBERT J., *Geophys. J. Int.*, **166** (2006) 97.
- [14] RAVELET F., MARIÉ L., CHIFFAUDEL A. and DAVIAUD F., *Phys. Rev. Lett.*, **93** (2004) 164501.
- [15] MUJICA N. and LATHROP D., *J. Fluid Mech.*, **551** (2006) 49.
- [16] BUSSE F., *J. Geophys.*, **43** (1977) 441.
- [17] Y. PONTY *et al.*, *Phys. Rev. Lett.*, **99** (2007) 224501.
- [18] KUANG W., JIANG W. and WANG T., *Geophys. Res. Lett.*, **35** (2008) L14204.
- [19] GROTE E. and BUSSE F. H., *Fluid Dyn. Res.*, **28** (2001) 349.
- [20] BUSSE F. H. and SIMITEV R., *Geophys. Astrophys. Fluid Dyn.*, **100** (2006) 341.
- [21] TILGNER A., *Int. J. Num. Meth. Fluids*, **30** (1999) 713.
- [22] KUTZNER C. and CHRISTENSEN U., *Phys. Earth Planet. Inter.*, **131** (2002) 29.
- [23] SREENIVASAN B. and JONES C. A., *Geophys. J. Int.*, **164** (2006) 467.